

Gradient Flow of Energy: A General and Efficient Approach for Entity Alignment Decoding

Yuanyi Wang¹, Haifeng Sun¹, Lei Zhang², Bo He¹, Wei Tang¹, Jingyu Wang¹,
Qi Qi¹, and Jianxin Liao¹

¹ State Key Laboratory of Networking and Switching Technology,
Beijing University of Posts and Telecommunications, Beijing, China
{wangyuanyi,hfsun,hebo,tangocean,wangjingyu,qiqi8266}@bupt.edu.cn,
² China Unicom, Beijing, China.
zhangl83@chinaunicom.cn

Abstract. Entity alignment (EA), a pivotal process in integrating multi-source Knowledge Graphs (KGs), seeks to identify equivalent entity pairs across these graphs. Most existing approaches regard EA as a graph representation learning task, concentrating on enhancing graph encoders. However, the decoding process in EA - essential for effective operation and alignment accuracy - has received limited attention and remains tailored to specific datasets and model architectures, necessitating both entity and additional explicit relation embeddings. This specificity limits its applicability, particularly in GNN-based models. To address this gap, we introduce a novel, generalized, and efficient decoding approach for EA, relying solely on entity embeddings. Our method optimizes the decoding process by minimizing Dirichlet energy, leading to the gradient flow within the graph, to maximize graph homophily. The discretization of the gradient flow produces a fast and scalable approach, termed **Triple Feature Propagation (TFP)**. TFP innovatively generalizes adjacency matrices to multi-views matrices: *entity-to-entity*, *entity-to-relation*, *relation-to-entity*, and *relation-to-triple*. The gradient flow through generalized matrices enables TFP to harness the multi-view structural information of KGs. Rigorous experimentation on diverse public datasets demonstrates that our approach significantly enhances various EA methods. Notably, the approach achieves these advancements with less than 6 seconds of additional computational time, establishing a new benchmark in efficiency and adaptability for future EA methods.

Keywords: Entity Alignment · Knowledge Graphs · Dirichlet Energy · Graph Homophily · Decoder · Triple Feature Propagation.

1 Introduction

Entity alignment (EA), essential for integrating Knowledge Graphs (KGs), remains a significant challenge in the Semantic Web [7, 38]. This process, aimed at identifying corresponding entities across distinct KGs, typically involves encoding and decoding phases (in Fig.1 (1)). Current EA methods depend on initial

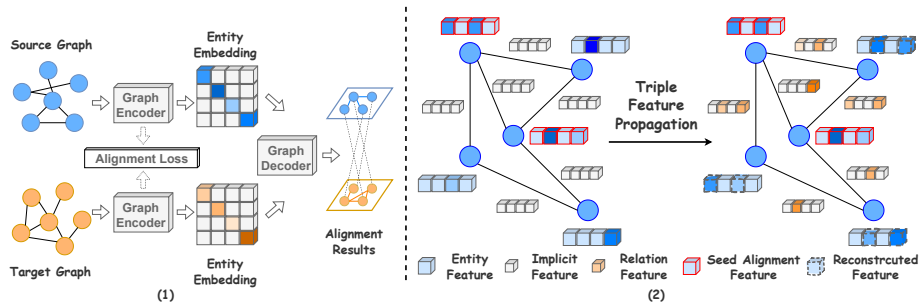


Fig. 1: (1) The architecture of existing EA methods that involve the encoding and decoding phase. (2) TFP maintains seed alignment features while reconstructing other entity features. It decodes relation features, not directly provided by encoders, to make them explicit based on entity features.

alignments to train encoders for generating entity and, optionally, relation embeddings, which are then decoded to establish alignments.

Recently, EA is approached as a graph representation learning task, with emphasis on improving graph encoders, which fall into two main categories: translation-based models, such as TransE [2] and its variants [3, 9], and Graph Neural Networks (GNN)-based models, like GCN-Align [39], MRAEA [19], and Dual-AMN [18]. The former views relation embeddings as translation vectors between entities, while the latter aggregates neighboring embeddings to generate entity representations. Recent efforts have enhanced encoder training with additional information, yielding superior alignment accuracy in models like TEA-GNN [43] and DualMatch [16], which utilize temporal data, and UMAEA [4] and DESAlign [37], which incorporate images and entity names.

However, despite advancements in encoders, decoder research [35] remains underdeveloped, often constrained by dataset and model specifics. Commonly used, the *greedy search* decoder, is flawed by potentially aligning multiple entities to a single target, contradicting EA’s one-to-one mapping principle. Alternative methods like CSLS [13] and global alignment strategies [45, 52] attempt to address these limitations using algorithms such as the Hungarian [12] or Sinkhorn [6], yet without deeply leveraging KG structural properties. DATTI [21] progresses by employing Third-order Tensor Isomorphism for decoding, but its utility is restricted by the necessity for explicit relation embeddings, which many GNN-based encoders do not provide.

In light of these considerations, we propose that an efficient EA decoder should fulfill two key criteria: (i) the ability to exploit the structural information inherent in KGs, and (ii) the capacity to generalize across various types of graph encoders. Regarding the first criterion, it is essential to consider both the distribution characteristics of the graph representations generated by the encoders and the intrinsic structural information of the KGs during the decoding phase. For the second criterion, the approach should be adaptable to both translation-based and GNN-based encoder architectures. A notable distinction lies in the fact that

translation-based encoders typically produce explicit relation embeddings along with entity embeddings, whereas most GNN-based encoders primarily generate entity embeddings. Despite this, some GNN-based encoders [18] do extract explicit relation embeddings based on entity embedding, underscoring that entity embeddings are central to the graph representation.

In this work, we propose a novel EA decoding approach, Triple Feature Propagation (TFP), that innovatively employs the structural information of KG to reconstruct the entity embeddings by maximizing homophily through minimizing the Dirichlet energy of the entity embedding. Unlike existing methods [8, 10], TFP utilizes the gradient flow of Dirichlet energy for efficient information propagation across various graph encoder types, avoiding the need for supplementary information. This approach is a multi-view propagation-based entity embedding reconstruction step, i.e., the decoding process, subsequent to the graph encoding phase. Specifically, TFP generalizes the traditional adjacency matrix to multi-view matrices—*entity-to-entity*, *entity-to-relation*, *relation-to-entity*, and *relation-to-triple*—to depict a comprehensive representation of KG structures. It combines these matrices and minimizes Dirichlet energy to initiate a gradient flow within the graph, facilitating effective information propagation. The propagation reconstructs the entity feature and generates the explicit relation feature (in Fig.1(2)). TFP establishes a fast, scalable, and theoretical decoding solution.

Our evaluation of TFP across both translation- and GNN-based encoders, incorporating six advanced EA methods, demonstrates performance gains across widely recognized public datasets. Remarkably, TFP enhances even state-of-the-art (SOTA) methods with minimal additional computational time, less than 6 seconds, setting a new benchmark for efficiency and adaptability in EA strategies.

Our contributions are multifaceted:

- (1) To comprehensively represent the KG structure, we generalize adjacency matrices through multi-view matrices for entity-to-entity, entity-to-relation, relation-to-entity, and relation-to-triple relationships.
- (2) We design TFP, a fast, general, and efficient decoding approach that combines multi-view matrices to reconstruct the entity embeddings to maximize homophily by minimizing the Dirichlet energy.
- (3) We offer a theoretical foundation for TFP through gradient flow theory. TFP is naturally generated through gradient flow of minimizing the Dirichlet energy.
- (4) Extensive experiments are conducted to demonstrate TFP can improve upon current EA methods only rely on entity embeddings with minimal computational cost, typically less than 6 seconds.

2 Related Work

Entity Alignment Encoders. EA is predominantly viewed as a graph representation learning endeavor, with encoders designed to intricately model KG structures [49]. Encoders fall into two main categories: translation-based, exemplified by TransE [2] and its variants [3, 9, 26], which emphasize embedding learning strategy; and GNN-based, which leverage a variety of GNN architectures to

produce entity embeddings. These include simple GCNs [39], multi-hop and relational GCNs [34, 48], graph attention networks [18, 31, 51], and self-supervised GCNs [14]. Innovations extend to semi-supervised [14, 19] and active learning approaches [1, 15, 50], plus the integration of additional information like entity attributes or temporal data [16, 30, 36, 41, 43, 44]. Our TFP decoding strategy aims to reconstruct entity representation via feature propagation, deriving from Dirichlet energy’s gradient flow to maximize homophily. TFP, adaptable across graph encoder types, enhances these encoders, including advanced models.

Entity Alignment Decoders. EA decoders traditionally aim at pairing entities from different KGs using learned embeddings. The *greedy search* algorithm [29, 47], though widely used, can produce multiple mappings for a single entity, conflicting with EA’s one-to-one mapping principle. Alternative methods like Cross-Domain Similarity Local Scaling (CSLS) [13] and the deferred acceptance algorithm [28] have sought to refine alignment accuracy. More recent efforts [45, 52] employ global alignment strategies, using algorithms such as the Hungarian [12] or Sinkhorn [6], yet often overlook KGs’ distinctive structural properties. DATTI [21] advances decoding by utilizing Third-order Tensor Isomorphism to capture structural information but is limited by its requirement for explicit relation embeddings, absent in many GNN-based models. TFP distinguishes itself by focusing on entity embeddings, fundamental to all encoder types, and establishes a fast and scalable decoding solution requiring only about 6 seconds, applicable across a wide range of encoder architectures.

3 Preliminary

Knowledge graph (KG), $\mathcal{G} = (\mathcal{E}, \mathcal{R}, \mathcal{T})$, stores the real-world knowledge in the form of \mathcal{T} , given a set of entities \mathcal{E} , a set of relations \mathcal{R} , and a set of triples $\mathcal{T} = \{(h, r, t) | h, t \in \mathcal{E}, r \in \mathcal{R}\}$, where h, t denote the head entity and the tail entity, r denotes the relation.

Definition 1. Entity Alignment (EA) aims to discover a one-to-one mapping $\Phi = \{(e_s, e_t) | e_s \in \mathcal{E}_s, e_t \in \mathcal{E}_t, e_s \equiv e_t\}$ between entities from a source KG $\mathcal{G}_s = (\mathcal{E}_s, \mathcal{R}_s, \mathcal{T}_s)$ to a target KG $\mathcal{G}_t = (\mathcal{E}_t, \mathcal{R}_t, \mathcal{T}_t)$, where \equiv signifying an equivalence relation between entities e_s and e_t .

For a simple directed graph $G = (V, E)$ with labels $y = \{y_i | i \in V\}$, where V represents the set of vertices and E the set of edges, the concept of graph homophily is crucial. Homophily indicates the likelihood of connected nodes sharing the same label. Formally, we define the homophily of a graph G as:

$$\mathcal{H}(G) = \mathbb{E}_{i \in V} \left[\frac{|\{j \in \mathcal{N}_i^{in} : y_i = y_j\}|}{|\mathcal{N}_i^{in}|} \right] \quad (1)$$

Here, $|\{j \in \mathcal{N}_i^{in} : y_i = y_j\}|$ quantifies the number of neighbors of node i in V sharing the same label y_i [25]. A graph G is considered homophilic if $\mathcal{H}(G) \approx 1$ and heterophilic if $\mathcal{H}(G) \approx 0$.

Definition 2. (Laplacian matrix.) We define the adjacency matrix of G as \mathbf{A} , the symmetrically normalized adjacency is represented by $\tilde{\mathbf{A}} = \mathbf{D}^{-\frac{1}{2}} \mathbf{A} \mathbf{D}^{-\frac{1}{2}}$, and the symmetrically normalized Laplacian matrix as $\mathbf{\Delta} = \mathbf{I} - \tilde{\mathbf{A}}$.

The concept of Dirichlet energy is often employed to measure the homophily in graph embeddings. We define it as follows:

Definition 3. (Dirichlet Energy.) Given the graph node embedding $\mathbf{X} \in \mathbb{R}^{N \times d}$, the graph homophily can be measured by the Dirichlet energy of \mathbf{X} :

$$\mathcal{L}(\mathbf{X}) = \text{tr}(\mathbf{X}^\top \mathbf{\Delta} \mathbf{X}) = \frac{1}{2} \sum_{i,j=1}^N a_{i,j} \left\| \frac{\mathbf{X}_i}{\sqrt{\mathbf{D}_{i,i} + 1}} - \frac{\mathbf{X}_j}{\sqrt{\mathbf{D}_{j,j} + 1}} \right\|_2^2 \quad (2)$$

4 Methodology

In this section, we introduce our proposed decoding approach, Triple Feature Propagation (TFP). Since the symmetrically Laplacian matrix $\mathbf{\Delta}$ is derived from the undirected adjacency, which captures the entity-to-entity structure, we initially focus on gradient flow within this special situation before extending the approach to the generalized adjacency matrix. Before the decoding process, we need to train an encoder to get the entity embedding as the initial feature $\mathbf{X}^{(0)} = \text{Enocder}(\mathcal{G}) \in \mathbb{R}^{|\mathcal{E}| \times d}$. The process of TFP is shown in Fig.2.

4.1 Gradient Flow

Given seed alignment entity features x_s , our objective is to reconstruct the features x_o of other entities by minimizing the Dirichlet energy $\mathcal{L}(\mathbf{X})$. We designate the set of seed alignment entities as $\mathcal{E}_s \subseteq \mathcal{E}$, with the remaining entities denoted by $\mathcal{E}_o = \mathcal{E} \setminus \mathcal{E}_s$. The entities are ordered such that:

$$\mathbf{X} = \begin{pmatrix} \mathbf{x}_s \\ \mathbf{x}_o \end{pmatrix}, \quad \mathbf{\Delta} = \begin{pmatrix} \mathbf{\Delta}_{ss} & \mathbf{\Delta}_{so} \\ \mathbf{\Delta}_{os} & \mathbf{\Delta}_{oo} \end{pmatrix} \quad (3)$$

The gradient flow of Dirichlet energy results in the graph heat equation [5], with seed alignment features remaining stationary. This is expressed as:

$$\frac{d\mathbf{X}(t)}{dt} = -\nabla_{\mathbf{x}} \mathcal{L}(\mathbf{X}(t)) = -\mathbf{\Delta} \mathbf{X}(t) \quad (4)$$

By integrating the boundary condition $\mathbf{x}_s(t) = \mathbf{x}_s$, the solution to this heat equation provides the required decoding process. The gradient flow for seed alignments is $\mathbf{0}$, leading to the compact expression:

$$\frac{d}{dt} \begin{pmatrix} \mathbf{x}_s(t) \\ \mathbf{x}_o(t) \end{pmatrix} = - \begin{pmatrix} \mathbf{0} & \mathbf{0} \\ \mathbf{\Delta}_{os} & \mathbf{\Delta}_{oo} \end{pmatrix} \begin{pmatrix} \mathbf{x}_s \\ \mathbf{x}_o(t) \end{pmatrix} = \begin{pmatrix} \mathbf{0} \\ -\mathbf{\Delta}_{os} \mathbf{x}_s - \mathbf{\Delta}_{oo} \mathbf{x}_o(t) \end{pmatrix} \quad (5)$$

Given the positive semi-definite nature of the graph Laplacian matrix, Dirichlet energy \mathcal{L} is convex, and its global minimizer is the solution to the gradient equation $\nabla \mathcal{L}(\mathbf{X}(t)) = 0$. The solution in equation (5) can be expressed as:

$$\frac{d\mathbf{x}_o(t)}{dt} = -\Delta_{os}\mathbf{x}_s - \Delta_{oo}\mathbf{x}_o(t) = \mathbf{0} \quad (6)$$

Therefore, we present the following proposition:

Proposition 1. (*Existence of the solution.*) *The matrix Δ_{oo} is non-singular, allowing the reconstruction of other entity features \mathbf{x}_o using seed alignment entity features \mathbf{x}_s as $\mathbf{x}_o(t) = -\Delta_{oo}^{-1}\Delta_{os}\mathbf{x}_s$.*

Proof. Please refer to Appendix A. □

However, solving this system of linear equations is computationally intensive, with a complexity of $O(|\mathcal{E}_o|^3)$ for matrix inversion, rendering it impractical for large graphs. Therefore, we discretize the process to tackle this challenge.

Remark. This special gradient flow in TFP is generalized to directed graphs, distinguishing it from FP [27] on undirected graphs.

4.2 Discretization Strategy

To tackle the computational challenges, we discretize the heat equation (5) and adopt an iterative approach for its resolution. By approximating the temporal derivative as a forward difference and discretizing time t with fixed steps ($t = hk$ for step size $h > 0$ and $k = 1, 2, \dots$), we employ the implicit Euler scheme:

$$\mathbf{X}^{(k+1)} = \mathbf{X}^{(k)} + h \frac{d\mathbf{X}(t)}{dt} \mathbf{X}^{(k)} \quad (7)$$

Incorporating the heat equation (4), the explicit Euler scheme is subsequently defined as:

$$\mathbf{X}^{(k+1)} = \begin{pmatrix} \mathbf{I} & \mathbf{0} \\ -h\Delta_{os} & \mathbf{I} - h\Delta_{oo} \end{pmatrix} \mathbf{X}^{(k)} \quad (8)$$

When focusing on the special case of $h = 1$, we can use the following observation to rewrite the iteration formula.

$$\tilde{\mathbf{A}} = \mathbf{I} - \Delta = \begin{pmatrix} \mathbf{I} - \Delta_{ss} & -\Delta_{so} \\ -\Delta_{os} & \mathbf{I} - \Delta_{oo} \end{pmatrix} \quad (9)$$

$$\mathbf{X}^{(k+1)} = \begin{pmatrix} \mathbf{I} & \mathbf{0} \\ \tilde{\mathbf{A}}_{os} & \tilde{\mathbf{A}}_{oo} \end{pmatrix} \mathbf{X}^{(k)} \quad (10)$$

This Euler scheme serves as a gradient descent for the Dirichlet energy, reducing the energy and smoothing the features. The approximation of this solution in this case is formalized as follows:

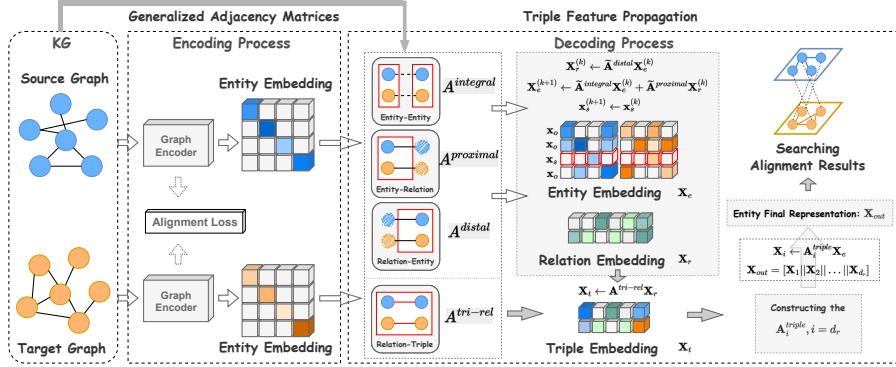


Fig. 2: The illustration of Triple Feature Propagation.

Proposition 2. (Approximation of the solution.) *With the iterative reconstruction solution as delineated in equation (10), and considering a sufficiently large iteration count N , the entity features will approximate the results of feature propagation as follows:*

$$\mathbf{X}^{(N)} \approx \begin{pmatrix} \mathbf{x}_s \\ \Delta_{oo}^{-1} \tilde{\mathbf{A}}_{os} \mathbf{x}_s \end{pmatrix} \quad (11)$$

Proof. Please refer to Appendix B. \square

The update process in Equation (10) equates to initially multiplying the entity features \mathbf{X} by the matrix $\tilde{\mathbf{A}}$, followed by resetting the seed alignment features to their original values. This results in a highly scalable and straightforward strategy for reconstructing other entity features:

$$\mathbf{X}^{(k+1)} \leftarrow \tilde{\mathbf{A}} \mathbf{X}^{(k)}; \quad \mathbf{x}_s^{(k+1)} \leftarrow \mathbf{x}_s^{(k)} \quad (12)$$

4.3 Generalized Adjacency Matrices

Our discussion has thus far established that the gradient flow of Dirichlet energy facilitates feature reconstruction within basic graph structures. However, KGs extend beyond the realm of simple directed graphs represented by an adjacency matrix \mathbf{A} . KGs encompass a richer structure, with triples $\mathcal{T} = \{(h, r, t), |h, t \in \mathcal{E}, r \in \mathcal{R}\}$, highlighting entity-to-entity ($h-t$), entity-to-relation ($h-r$), relation-to-entity ($r-t$), and relation-to-triple ($r-\mathcal{T}$). These perspectives encapsulate key meta-structures in KGs:

- 1. Entity-to-Relation.** Beyond the conventional adjacency matrix, the (h, r) pairs in triples provide a unique structural perspective, indicating directional links from head entity h to relation r . This directionality is fundamental and unidirectional. For instance, in the triple $(London, CapitalOf, England)$, the entity $[England]$ is connected to $[London]$ via the relation $[CapitalOf]$, but

not in reverse. Similar to the adjacency matrix \mathbf{A} , we define an *entity to relation* matrix $\mathbf{A}^{proximal} \in \mathbb{R}^{|\mathcal{E}| \times |\mathcal{R}|}$ based on the (h, r) pairs as:

$$\exists e \in \mathcal{E} : \mathbf{A}_{i,j}^{proximal} = 1, (h_i, r_j, e) \in \mathcal{T} \quad \mathbf{A}_{i,j}^{proximal} = 0, (h_i, r_j, e) \notin \mathcal{T} \quad (13)$$

2. **Relation-to-Entity.** This category, akin to *entity to relation*, encompasses directed and irreversible information. It underscores the more distant positional relationships between relations and tail entities. The resulting structural matrix, $\mathbf{A}^{distal} \in \mathbb{R}^{|\mathcal{R}| \times |\mathcal{E}|}$, is defined as:

$$\exists e \in \mathcal{E} : \mathbf{A}_{i,j}^{distal} = 1, (e, r_i, t_j) \in \mathcal{T} \quad \mathbf{A}_{i,j}^{distal} = 0, (e, r_i, t_j) \notin \mathcal{T} \quad (14)$$

3. **Entity-to-Entity.** Representing the fundamental structural category, this is similar to the adjacency matrix \mathbf{A} . While \mathbf{A} provides a solid foundation and is rich in spectral properties, it is insufficient to fully represent KG structures. For example, the triples $(London, CapitalOf, England)$ are structurally distinct with $(London, LocateIn, England)$ in KGs, yet a traditional adjacency matrix treats them identically as they both represent *London* connects *English*, representing $\mathbf{A}_{i,j} = 1$. To better represent relationships between entities, we extend the adjacency matrix to $\mathbf{A}^{integral} \in \mathbb{R}^{|\mathcal{E}| \times |\mathcal{E}|}$:

$$\exists r \in \mathcal{R} : \quad \mathbf{A}_{i,i}^{integral} = |\mathcal{T}_{e_i}| \\ \mathbf{A}_{i,j}^{integral} = |\mathcal{T}_{(h_i, t_j)}|, (h_i, r, t_j) \in \mathcal{T} \quad \mathbf{A}_{i,j}^{integral} = 0, (h_i, r, t_j) \notin \mathcal{T} \quad (15)$$

$|\mathcal{T}_{e_i}|$ denotes the number of triples involving entity e_i , and $|\mathcal{T}_{(h_i, t_j)}|$ indicates the count of triples with the pair (h_i, t_j) .

4. **Relation-to-Triple.** As discussed before, the knowledge in KG is stored in the triple $\mathcal{T} = \{(h, r, t), |h, t \in \mathcal{E}, r \in \mathcal{R}\}$, which is the core representation of the KG structure. The unique role of relation r within triple \mathcal{T} motivates the extension of the adjacency matrix to the triple level through relation r . We introduce the adjacency matrix $\mathbf{A}^{tri-rel} \in \mathbb{R}^{|\mathcal{T}| \times |\mathcal{R}|}$, defined as:

$$\mathbf{A}_{i,j}^{tri-rel} = 1, r_j \in \mathcal{T}_i \quad \mathbf{A}_{i,j}^{tri-rel} = 0, r_j \notin \mathcal{T}_i \quad (16)$$

Note. The *entity-to-triple* matrix is also considered. This matrix is considered to represent *entity-entity-triple* relationships for head (h) and tail (t) entities connections in \mathcal{T} . However, we find that these connections are already encapsulated within the *entity-to-entity* matrix $\mathbf{A}^{integral}$. This matrix, $\mathbf{A}^{integral}$, which details connections between head h and tail t entities, effectively doubles as an *entity-to-triple* representation.

Having established that the gradient flow of Dirichlet energy facilitates reconstruction based on common adjacency relationships as outlined in equation (10), we extend this concept to the specialized adjacency matrices of KGs. We assume that the normalized form of $\mathbf{A}^{proximal}$, \mathbf{A}^{distal} , and $\mathbf{A}^{integral}$, which are similar to graph Laplacian, representing different facets of KG structure, possess analogous spectral properties. The experimental results confirm our view.

Consequently, the gradient flow should yield comparable solutions across these matrices. We denote their normalized form $\tilde{\mathbf{A}}^{k,k=\{proximal,distal,integral\}}$

$$\tilde{\mathbf{A}}_i^k = \frac{\mathbf{A}_i^k}{\sum_{j=0}^{number\ of\ column} \mathbf{A}_{i,j}^k} \quad (17)$$

4.4 Triple Feature Propagation

Utilizing the gradient flow of Dirichlet energy on these categories of KG structure, we derive a natural and straightforward generalized propagation strategy. The propagation process is articulated through the following equations:

$$\mathbf{X}_r^{(k)} = \tilde{\mathbf{A}}^{distal} \mathbf{X}_e^{(k)} \quad (18)$$

$$\mathbf{X}_e^{(k+1)} = \tilde{\mathbf{A}}^{integral} \mathbf{X}_e^{(k)} + \tilde{\mathbf{A}}^{proximal} \mathbf{X}_r^{(k)} \quad (19)$$

$$\mathbf{x}_s^{(k+1)} = \mathbf{x}_s^{(k)} \quad (20)$$

Here, $\mathbf{X}_e^{(i)}$, $1 \leq i \leq k + 1$, denotes the entity features, initially derived from the graph encoder as $\mathbf{X}_e^{(0)}$. \mathbf{X}_r represents the implicit relation features generated through the propagation strategy. To comprehensively capture the evolving entity and relation information across iterations, we aggregate entity features from each step through concatenation, resulting in the entity feature as follows:

$$\mathbf{X}_e = [\mathbf{X}^{(0)} || \mathbf{X}^{(1)} || \dots || \mathbf{X}^{(k)}] \quad (21)$$

We notice that our process explicitly captures the implicit relation feature \mathbf{X}_r , serving as an essential intermediary. By leveraging the *triple-to-relation* matrix, we further refine \mathbf{X}_r . We use a hyper-sphere independent random projection to reduce the dimension of \mathbf{X}_r to d_r , following the method outlined in [23]. This step enables the creation of the triple feature \mathbf{X}_t .

$$\mathbf{X}_r = \text{ranp}(\mathbf{X}_r) \in \mathbb{R}^{|\mathcal{R}| \times d_r} \quad (22)$$

$$\mathbf{X}_t = \mathbf{A}^{tri-rel} \mathbf{X}_r \quad (23)$$

Our method enables the representation of the KG structure as a three-dimensional tensor $\mathbf{A}^{triple} \in \mathbb{R}^{|\mathcal{E}| \times |\mathcal{E}| \times d_r}$, rather than the traditional adjacency matrix. The tensor is defined as:

$$\mathbf{A}_{h,t}^{triple} = \mathbf{X}_t(h, r, t), (h, t) \in \mathcal{T} \quad \mathbf{A}_{h,t}^{triple} = \mathbf{0}, (h, t) \notin \mathcal{T} \quad (24)$$

Here, $\mathbf{X}_t(h, r, t)$ represents the feature of triple (h, r, t) in \mathbf{X}_t . The KG structure is encapsulated in d_r slices as $\mathbf{A}_1^{triple}, \dots, \mathbf{A}_{d_r}^{triple} \in \mathbb{R}^{|\mathcal{E}| \times |\mathcal{E}|}$. Parallel to the relation feature, the entity feature \mathbf{X}_e is also scaled through hyper-sphere independent random projection to d_e dimension. The propagation process is based on the final entity features \mathbf{X}_e , allowing for the continuation of gradient flow from the triple

perspective. Since each \mathbf{A}_i^{triple} represents a segmented view of the overall \mathbf{A}^{triple} , their concatenation is essential to compile the comprehensive final feature.

$$\mathbf{X}_i = \mathbf{A}_i^{triple} \mathbf{X}_e, i = 1, \dots, d_r \quad (25)$$

$$\mathbf{X}_{out} = [\mathbf{X}_1 || \mathbf{X}_2 || \dots || \mathbf{X}_{d_r}] \quad (26)$$

TFP’s implementation is outlined in Algorithm 1. To identify alignment results, we adopt an approach from [21, 23] that frames the search as an assignment problem, moving beyond traditional Euclidean or cosine similarity calculations. This method upholds the one-to-one matching constraint and facilitates the use of the Sinkhorn operator [6] for faster computation. Detailed procedures are described in Appendix C.

Algorithm 1 TFP

Input: The embedding $\mathbf{X}^{(0)}$ from encoder, the triples \mathcal{T} , iteration number K , dimension d_r .
Output: The reconstructed feature \mathbf{X}_{out} .
 1: Initialize $\tilde{\mathbf{A}}^{proximal}$, $\tilde{\mathbf{A}}^{distal}$, $\tilde{\mathbf{A}}^{integral}$, and $\mathbf{A}^{tri-rel}$ through the triples \mathcal{T} .
 2: **for** $k = 1 \rightarrow K$ **do**
 3: $\mathbf{X}_r^{(k)} \leftarrow \tilde{\mathbf{A}}^{distal} \mathbf{X}_e^{(k)}$
 4: $\mathbf{X}_e^{(k+1)} \leftarrow \tilde{\mathbf{A}}^{integral} \mathbf{X}_e^{(k)} + \tilde{\mathbf{A}}^{proximal} \mathbf{X}_r^{(k)}$
 5: $\mathbf{x}_s^{(k+1)} \leftarrow \mathbf{x}_s^{(k)}$
 6: **end for**
 7: $\mathbf{X}_r \leftarrow random_projection(\mathbf{X}_r^{(K)}, d_r)$
 8: $\mathbf{X}_t \leftarrow \mathbf{A}^{tri-rel} \mathbf{X}_r$
 9: Generate \mathbf{A}_i^{triple} through \mathbf{X}_t .
 10: $\mathbf{X}_i \leftarrow \mathbf{A}_i^{triple} \mathbf{X}_e^{(K)}$
 11: $\mathbf{X}_{out} \leftarrow [\mathbf{X}_1 || \mathbf{X}_2 || \dots || \mathbf{X}_{d_r}]$
 12: **return** \mathbf{X}_{out}

Table 1: Execution time (seconds) of EA methods using TFP on DBP and SRPRS, where TFP(C) / (G) denotes CPU / GPU execution.

Time/s	Translation-based		GNN-based	
	DBP15K	SRPRS	Time/s	DBP15K SRPRS
AlignE	2087	1190	MRAEA	1743 558
TFP(C)	13.9	8.1	TFP(C)	16.6 10.6
TFP(G)	4.8	4.2	TFP(G)	5.9 4.6
RSN	3659	1279	RREA	323 276
TFP(C)	14.2	9.2	TFP(C)	16.3 11
TFP(G)	4.8	3.7	TFP(G)	5.7 3.8
TransEdge	1625	907	DualAMN	177 163
TFP(C)	12.9	8.7	TFP(C)	17.7 11.4
TFP(G)	4.7	3.6	TFP(G)	5.1 4.6

5 Experiments

To thoroughly assess the proposed Triple Feature Propagation method, our experiments target the following research questions:

1. Can TFP effectively generalize across different graph encoders and integrate with structural-based state-of-the-art methods?
2. How does TFP’s performance evolve across iterations when applied to different encoders on various datasets?
3. How does TFP’s time efficiency compare to that of encoders?
4. How does TFP perform when additional information is integrated, compared to other textual EA methods?

5.1 Experimental Settings

Our experimental setup includes details on datasets, baselines and evaluation metrics, and implementation details.

Datasets: We utilize two widely recognized datasets to test our decoding algorithm: (1) DBP15K [30] comprises three cross-lingual subsets from multilingual

DBpedia. Each subset contains 15,000 entity pairs. **(2)** SRPRS [9]. Similar to DBP15K in terms of the number of entity pairs but with fewer triples. For consistency with prior research [3, 39], we use a 30/70 split of pre-aligned entity pairs for training and testing encoders, respectively. Results are averaged over five independent runs. The more details have been provided in Appendix D.

Baseline and Evaluation Metrics: **(1)** Our evaluation includes six prominent EA encoder methods, divided into GNN-based—MRAEA [19], RREA [20], Dual-AMN [18] (with Dual-AMN as the structural SOTA)—and translation-based—AlignE [32], RSN [9], and TransEdge [33] (with TransEdge as the premier in its class). **(2)** For decoding baselines, we benchmark against the Hungarian algorithm [12], which is the prominent solution in previous work [45], and the SOTA of EA decoder, DATTI [21]. **(3)** Following most previous works [11, 49], our evaluation employs cosine similarity for EA and H@k and MRR metrics for a thorough evaluation. Details about these metrics can be found in Appendix E. **Note:** In our primary experiments, we utilize six encoders that only focus on structural information—the core information of EA tasks. Although some recent methods outperform these by integrating additional information, such as textual attributes, we also explore these situations in Section 5.5 for a broader evaluation. Comparative methods are detailed in Table.3.

Implementaion Details: The output dimensions d and other hyper-parameters of all encoders adhere to their original settings in their papers: Dual-AMN ($d = 768$), RREA($d = 600$), MRAEA ($d = 600$), AlignE ($d = 75$), RSN ($d = 256$), and TransEdge ($d = 75$). The iteration k is set to their best results, which details described in section 5.3. Other hyper-parameters remain the same for all datasets and methods: relation scale dimension $d_r = 512$, entity scale dimension $d_e = 16$. All experiments are conducted on a PC with an NVIDIA RTX A6000 GPU and an Intel Xeon Gold 6248R CPU.

5.2 Main Results (Q1)

The primary experimental results are summarized in Table 2. Among the evaluated six encoders, Dual-AMN demonstrates superior performance across all datasets, underscoring the efficacy of GNN encoders. Interestingly, TransEdge shows notable success on the DBP15K dataset but underperforms on SRPRS. This can be attributed to TransEdge’s reliance on existing edge semantic information for entity dependency capture, a feature less prevalent in the sparser KGs like SRPRS. Conversely, GNN-based models exhibit robust performance on sparse graphs, highlighting their aptitude for handling sparse topologies.

GNN-based encoders: Our TFP approach consistently improves performance across all datasets, even when enhancing the SOTA structure-based Dual-AMN method. On $DBP15KFR - EN$, TFP achieves gains of 2.25% in Hits@1 and 2.02% in MRR, and on $SRPRSFR - EN$, it increases by 1.28% in Hits@1 and 1.19% in MRR. Unlike the decoder DATTI, which is limited to encoders producing both entity and relation embeddings, TFP is applicable to any encoder, even those only generating explicit entity embeddings. These results validate three

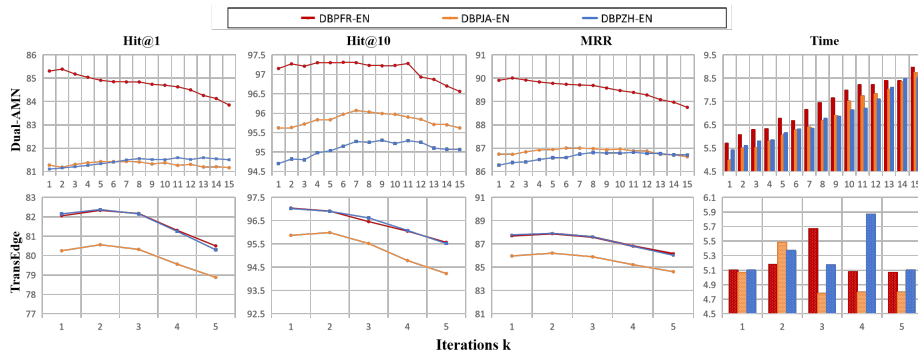


Fig. 3: Metrics and execution time (seconds) on DBP15K across iterations k .

key points: (i) the gradient flow of Dirichlet energy effectively reconstructs entity embeddings, facilitating feature propagation and preserving homophily; (ii) TFP’s effectiveness and generality across various GNN-based graph encoders; (iii) TFP’s utility and simplicity in augmenting structure-based methods.

Translation-based encoders: TFP significantly boosts the performance of translation-based EA encoders, effectively capturing multi-view structural information through the gradient flow to maximize the homophily. Notably, TFP improves AlignE’s performance by 28.87% in Hits@1 on the DBP15K_{JA-EN} dataset and by 25.8% on the SRPRS_{DE-EN} dataset. For the best translation-based encoder, TransEdge, TFP still achieves substantial enhancements, including at least a 7.01% increase in Hits@1 on DBP15K and 15.22% on SRPRS. These findings demonstrate TFP’s effectiveness and general applicability to translation-based encoders. Particularly, TFP’s significant improvement on the SRPRS dataset indicates its capability to bridge gaps in sparse KG topology understanding, an area where translation-based EA encoders typically struggle.

5.3 Exploratory Analysis (Q2)

In this subsection, we delve into the iterative performance of TFP when using Dual-AMN and TransEdge encoders on the DBP15K. The results, depicting TFP’s behavior across different iteration counts k , are illustrated in Figure 5.3.

Performance with Dual-AMN Encoder. Dual-AMN stands out in the DBP15K dataset for its performance in Hit@ k and MRR metrics. TFP’s iteration-dependent performance shows a typical increase followed by a plateau, and sometimes a decrease due to over-smoothing. For example, TFP peaks at $k = 11$ iterations on DBPZH-EN before stabilizing. However, Hit@10 initially decreases, then stabilizes, showing convergence despite random fluctuations. TFP shows quick convergence and notable improvements on DBPFR-EN, benefiting from its diverse topological structures [30]. Time analysis indicates that while computational time increases with iterations, it remains under 10 seconds even at $k = 15$, which is minor compared to the encoder’s training time.

Table 2: Main experimental results on DBP15K and SRPRS datasets. All results and initial embeddings were derived using official code with default hyper-parameters. "Improv." indicates the percentage improvement of TFP over EA encoder results. The Hungarian algorithm (Hun) produces only one aligned pair per entity, thus only Hits@1 is reported. DATTI cannot decode MRAEA and RREA, as it requires both entity and relation embeddings, whereas these encoders provide only entity embeddings.

Datasets		DBP _{FR-EN}			DBP _{JA-EN}			DBP _{ZH-EN}			SRPRS _{FR-EN}			SRPRS _{DE-EN}			
Model	H@1	H@10	MRR	H@1	H@10	MRR	H@1	H@10	MRR	H@1	H@10	MRR	H@1	H@10	MRR		
GNL-based	MRAEA	71.63	94.28	80.02	68.7	93.19	77.66	68.7	92.94	77.43	43.44	75.1	53.85	56.18	51.47	64.87	
	+Hun	80.33	-	-	76.54	-	-	78.04	-	-	45.29	-	-	58.70	-	-	
	+DATTI	-	-	-	-	-	-	-	-	-	-	-	-	-	-	-	
	+TFP	75.45	95.87	83.04	74.26	94.98	82.08	74.4	94.54	81.82	46.06	75.55	55.89	58.83	81.89	66.78	
	Improv.	5.3%	1.7%	3.8%	8.1%	1.9%	5.7%	8.3%	1.7%	5.7%	6.0%	0.6%	3.8%	4.7%	59.1%	2.9%	
	RREA	73.4	94.8	81.36	70.59	94.13	79.11	70.73	93.21	78.97	42.96	73.96	53.41	56.74	81.24	65.18	
	+Hun	80.42	-	-	78.44	-	-	78.69	-	-	45.68	-	-	58.96	-	-	
	+DATTI	-	-	-	-	-	-	-	-	-	-	-	-	-	-	-	
	+TFP	80.79	96.98	86.79	78.83	96.00	85.23	79.43	95.45	85.35	47.23	75.60	56.67	59.98	82.33	67.80	
	Improv.	10.1%	2.3%	6.7%	11.7%	2.0%	7.7%	12.3%	2.4%	8.1%	9.9%	2.2%	6.1%	5.7%	1.3%	4.0%	
GNL-based	DualAMN	83.43	96.19	88.14	80.31	94.69	85.57	80.39	93.68	85.29	48.28	75.51	57.34	61.2	81.91	68.3	
	+Hun	83.87	-	-	80.39	-	-	80.12	-	-	48.32	-	-	61.15	-	-	
	+DATTI	87.30	97.90	91.30	83.60	96.90	88.40	83.50	95.30	88.00	49.50	76.00	58.30	62.30	82.20	69.10	
	+TFP	85.31	97.26	89.92	81.26	95.85	86.82	81.64	95.24	86.84	48.90	76.28	58.02	61.84	82.61	69.01	
	Improv.	2.3%	1.1%	2.0%	1.2%	1.2%	1.5%	1.6%	1.7%	1.8%	1.3%	1.0%	1.2%	1.0%	0.9%	1.0%	
	Translation-based	AlignE	53.36	86.55	64.93	50.12	83.91	61.58	50.96	82.3	61.7	34.33	65.44	44.68	44.07	69.43	52.7
		+Hun	64.16	-	-	58.41	-	-	60.37	-	-	37.24	-	-	50.15	-	-
		+DATTI	58.55	85.96	68.01	55.62	82.80	64.80	57.50	82.70	66.15	39.15	69.12	49.19	53.55	75.59	61.29
		+TFP	68.45	91.96	76.81	64.59	90.77	73.76	66.98	89.78	74.89	42.11	71.80	51.98	55.44	78.61	63.48
		Improv.	28.3%	6.3%	18.3%	28.9%	8.2%	19.8%	31.4%	9.1%	21.4%	22.7%	9.7%	16.3%	25.8%	13.2%	20.5%
RSN		63.17	86.37	71.33	59.13	81.5	67.03	60.67	82.86	68.53	35.1	63.78	44.73	51.07	74.43	59.02	
+Hun		69.25	-	-	63.33	-	-	66.08	-	-	37.42	-	-	53.79	-	-	
+DATTI		72.00	91.80	79.00	68.60	89.50	75.90	72.10	90.30	78.50	40.70	69.40	50.20	55.90	78.20	63.70	
+TFP		77.79	92.45	83.73	73.53	91.97	80.04	75.44	91.71	81.33	44.32	73.22	53.97	59.27	81.14	66.84	
Improv.		23.1%	7.0%	17.4%	24.4%	12.8%	19.4%	24.3%	10.7%	18.7%	26.3%	14.8%	20.7%	16.1%	9.0%	13.2%	
Translation-based	TransEdge	76.9	93.97	83.03	74.66	92.93	81.1	76.19	92.16	81.81	40.81	67.66	49.73	55.65	75.3	64.28	
	+Hun	79.55	-	-	77.06	-	-	78.72	-	-	42.65	-	-	57.41	-	-	
	+DATTI	81.80	96.50	87.30	80.40	95.70	86.10	81.40	94.70	86.30	44.10	70.70	52.10	59.30	78.20	67.30	
	+TFP	82.36	96.90	87.91	80.52	95.96	86.19	81.53	95.21	86.50	49.03	75.22	56.49	64.12	81.70	70.95	
	Improv.	7.1%	3.1%	5.9%	7.8%	3.3%	6.3%	7.0%	3.3%	5.7%	20.1%	11.2%	13.6%	15.2%	8.5%	10.4%	

Analysis with TransEdge Encoder. TransEdge, a leading translation-based encoder, requires fewer iterations for TFP to converge and exhibit significant enhancements. Unlike Dual-AMN, TransEdge excels in capturing higher-level semantic information but falls short in detailing topological structures, a common trait among translation-based encoders. TFP effectively compensates for this limitation by reconstructing entity features that assimilate topological information from three distinct perspectives, thereby enriching the quality of entity features. This implies that during the encoding stage, structural noise due to model bias is minimal, reducing the need for extensive denoising during decoding. Interestingly, an inverse proportionality emerges between iteration count and time cost beyond $k = 2$, characterized by a diminishing time requirement with increasing iterations. Our comprehensive experimental analysis attributes this phenomenon to TFP's enhancement of homophily in relational features during the decoding phase leading to over-smoothing, particularly at higher iteration

counts. This augmentation results in sparser features as per equations (18) and (23), culminating in over-smoothing that, in turn, leads to a reduction in computational time due to the increased feature sparsity.

5.4 Time Complexity Analysis (Q3)

TFP operates through iterative sparse-to-dense matrix multiplications, positioned as the subsequent step after encoders. Adapting from [23], we streamline these multiplications in Eqs. (18) and (19) into the *sparse-dense-multiplications* form to sustain a computational complexity of $O(k(|\mathcal{T}|d_r + |\mathcal{E}|d_e))$. For Eqs. (23) and (25), Tensorflow’s sparse matrix multiplications are utilized, bringing the complexity down to approximately $O(|\mathcal{T}|d_r)$ and $O(|\mathcal{E}|d_e)$ respectively.

In Table 1, we present a detailed comparison of the time costs associated with the training and decoding phases (TFP) across six EA encoders, utilizing both CPU and GPU, on DBP15K and SRPRS datasets. Notably, the propagation step of TFP constitutes only a minor portion of the overall runtime, with the bulk of the time being allocated to the encoder training process. Remarkably, on a GPU, TFP’s execution time peaks at just 5.9 seconds. Even when operating on a CPU, TFP requires a maximum of merely 17.7 seconds. This duration is insignificant when contrasted with even the fastest encoder, Dual-AMN.

A comparative observation reveals that TFP’s application is expedited on translation-based encoders relative to GNN-based ones. This acceleration is attributable to the varying entity embedding dimensions discussed in Section 5.1. The output dimension for GNN-based encoders, particularly for MRAEA and Dual-AMN, is set at $d = 600$ and $d = 768$, respectively, which is larger than that of the translation-based encoders. This discrepancy in dimensionality directly influences the time efficiency of TFP, as demonstrated by the faster performance on translation-based models.

5.5 Additional Information (Q4)

Within the scope of EA, most experiments have largely focused on purely structural-based methods. However, some research [42,46] has introduced supplementary information (entity names) to refine EA performance. These advanced approaches typically employ machine translation systems or cross-lingual word embeddings to transition entity names into a cohesive semantic space, subsequently utilizing averaged pre-trained word embeddings to formulate initial features for both entities and relations. In this enhanced context, initial entity features $\mathbf{X}_e^{(0)}$ are pre-aligned, positioning these textual EA methods akin to decoding algorithms that emphasize topology and dependencies. Consequently, TFP is capable of fulfilling a similar role, akin to scenarios where seed alignment sets are absent.

To make fair comparisons with these textural-based EA methodologies, we adopted identical entity name translations and pre-trained word embeddings as delineated by Xu et al. [46]. We established two distinct scenarios for this assessment:

Table 3: Performances of textual EA methods, which make alignment by additional entity name. The results of baselines are collected from the original papers. TFP(Initial) represents directly using entity name (literal feature) as the initial entity feature and TFP(SEU) represents the initial features generated by SEU.

Datasets	DBP _{FR-EN}			DBP _{JA-EN}			DBP _{ZH-EN}			SRPRS _{FR-EN}			SRPRS _{DE-EN}		
	H@1	MRR	Time/s	H@1	MRR	Time/s	H@1	MRR	Time/s	H@1	MRR	Time/s	H@1	MRR	Time/s
GM-Align [46]	89.4	-	26328	73.9	-	26328	67.9	-	26328	57.4	60.2	13032	68.1	71.0	13032
RDGCN [41]	87.3	90.1	6711	76.3	76.3	6711	69.7	75.0	6711	67.2	71.0	886	77.9	82.0	886
HGCN [42]	76.6	81.0	11275	89.2	91.0	11275	72.0	76.0	11275	67.0	71.0	2504	76.3	80.1	2504
AttrGNN [17]	91.9	91.0	-	78.3	83.4	-	79.6	84.5	-	-	-	-	-	-	-
EPEA [40]	95.5	96.7	-	92.4	94.2	-	88.5	91.1	-	-	-	-	-	-	-
SEU [22]	98.8	99.2	17.0	95.6	96.9	16.2	90.0	92.4	16.2	98.2	98.6	9.6	98.3	98.7	9.8
LightEA [23]	99.5	99.6	15.7	98.1	98.7	14.8	95.2	96.4	15.2	98.6	98.9	11.2	98.8	99.1	11.4
TFP(Initial)	98.3	98.87	4.8	94.1	95.49	4.7	87.43	89.98	4.9	98.99	99.28	3.6	98.83	99.12	3.6
TFP(SEU)	99.05	99.4	4.9	96.21	97.19	4.7	90.51	92.63	5.1	98.55	98.95	3.7	98.57	98.95	3.8

- (i) TFP(Initial), which utilizes TFP as a standalone textual EA method on pre-aligned entity name features.
- (ii) TFP(SEU), which employs the textual EA method SEU as the encoder, with TFP acting as the decoder.

Table 3 delineates the performance metrics of TFP(Initial), TFP(SEU), and seven other baseline methods across the DBP15K and SRPRS datasets. Remarkably, TFP, as an unsupervised textual EA method, surpasses all other competitors on SRPRS and secures a near-top placement on DBP15K. Utilizing SEU as an encoder alongside TFP further elevates performance, nearing the benchmark of 100% accuracy. Notably, the comparative results of SEU, LightEA, and TFP exhibit formidable competitiveness, aligning more with propagation strategies than neural network paradigms. This indicates redundancy in current textual EA methodologies, suggesting that the complex neural networks and pre-aligned entity pairs may be unnecessary with pre-aligned initial features. Importantly, TFP achieves these results with significantly less time than other methods.

Despite demonstrating strong competitive prowess, TFP(SEU) exhibits a slight performance decrement compared to the use of initial entity name features exclusively. This can be attributed to the inherent similarities between SEU and TFP: both operate on propagation principles, ostensibly acting as smoothing strategies predicated on topological data assimilation. In scenarios involving sparse KGs, SEU’s ability to comprehensively capture topological nuances and facilitate entity embedding smoothing is significant. However, subsequent application of TFP may precipitate over-smoothing, which elucidates the observed performance discrepancy.

6 Conclusion

In this paper, we presented Triple Feature Propagation (TFP), an innovative, effective and theoretical approach for entity alignment decoding. TFP extends traditional adjacency matrices into multi-view matrices—encompassing entity-to-entity, entity-to-relation, relation-to-entity, and relation-to-triples relation-

ships—to reconstruct entity embeddings. This reconstruction, aimed at homophily maximization, is achieved by minimizing the Dirichlet energy, facilitating a natural feature propagation through gradient flow theory. Our experiments confirm TFP’s capability to improve the performance of various EA methods, with less than 6 seconds of additional computational time. This efficiency and general applicability make TFP a promising advancement in the field of entity alignment.

Supplemental Material Statement: The source code and constructed datasets are available at our repository: <https://github.com/wyy-code/TFP> The proofs of our proposition and other details are provided in the Appendix.

References

1. Berrendorf, M., Faerman, E., Tresp, V.: Active learning for entity alignment. In: Advances in Information Retrieval: 43rd European Conference on IR Research, ECIR 2021, Virtual Event, March 28–April 1, 2021, Proceedings, Part I 43. pp. 48–62. Springer (2021)
2. Bordes, A., Usunier, N., Garcia-Duran, A., Weston, J., Yakhnenko, O.: Translating embeddings for modeling multi-relational data. *Advances in neural information processing systems* **26** (2013)
3. Chen, M., Tian, Y., Yang, M., Zaniolo, C.: Multilingual knowledge graph embeddings for cross-lingual knowledge alignment. In: Proceedings of the 26th International Joint Conference on Artificial Intelligence. pp. 1511–1517 (2017)
4. Chen, Z., Guo, L., Fang, Y., Zhang, Y., Chen, J., Pan, J.Z., Li, Y., Chen, H., Zhang, W.: Rethinking uncertainly missing and ambiguous visual modality in multi-modal entity alignment. In: International Semantic Web Conference. pp. 121–139. Springer (2023)
5. Chung, F.: Spectral graph theory. In: CBMS Regional Conference Series in Mathematics. American Mathematical Society (1996)
6. Cuturi, M.: Sinkhorn distances: Lightspeed computation of optimal transport. *Advances in neural information processing systems* **26** (2013)
7. Dsouza, A., Yu, R., Windoffer, M., Demidova, E.: Iterative geographic entity alignment with cross-attention. In: International Semantic Web Conference. pp. 216–233. Springer (2023)
8. Fey, M., Lenssen, J.E., Morris, C., Masci, J., Kriege, N.M.: Deep graph matching consensus. In: International Conference on Learning Representations (2019)
9. Guo, L., Sun, Z., Hu, W.: Learning to exploit long-term relational dependencies in knowledge graphs. In: International conference on machine learning. pp. 2505–2514. PMLR (2019)
10. Heimann, M., Chen, X., Vahedian, F., Koutra, D.: Refining network alignment to improve matched neighborhood consistency. In: Proceedings of the 2021 SIAM International Conference on Data Mining (SDM). pp. 172–180. SIAM (2021)
11. Ji, S., Pan, S., Cambria, E., Marttinen, P., Yu, P.S.: A survey on knowledge graphs: Representation, acquisition, and applications. *IEEE Trans. Neural Networks Learn. Syst.* **33**(2), 494–514 (2022)
12. Kuhn, H.W.: The hungarian method for the assignment problem. *Naval research logistics quarterly* **2**(1-2), 83–97 (1955)

13. Lample, G., Conneau, A., Ranzato, M., Denoyer, L., Jégou, H.: Word translation without parallel data. In: International Conference on Learning Representations (2018)
14. Li, J., Song, D.: Uncertainty-aware pseudo label refinery for entity alignment. In: Proceedings of the ACM Web Conference 2022. pp. 829–837 (2022)
15. Liu, B., Scells, H., Zuccon, G., Hua, W., Zhao, G.: Activeea: Active learning for neural entity alignment. In: Proceedings of the 2021 Conference on Empirical Methods in Natural Language Processing. pp. 3364–3374 (2021)
16. Liu, X., Wu, J., Li, T., Chen, L., Gao, Y.: Unsupervised entity alignment for temporal knowledge graphs. In: Proceedings of the ACM Web Conference 2023. pp. 2528–2538 (2023)
17. Liu, Z., Cao, Y., Pan, L., Li, J., Chua, T.S.: Exploring and evaluating attributes, values, and structures for entity alignment. In: Proceedings of the 2020 Conference on Empirical Methods in Natural Language Processing (EMNLP). pp. 6355–6364 (2020)
18. Mao, X., Wang, W., Wu, Y., Lan, M.: Boosting the speed of entity alignment 10×: Dual attention matching network with normalized hard sample mining. In: Proceedings of the Web Conference 2021. pp. 821–832 (2021)
19. Mao, X., Wang, W., Xu, H., Lan, M., Wu, Y.: Mraea: an efficient and robust entity alignment approach for cross-lingual knowledge graph. In: Proceedings of the 13th International Conference on Web Search and Data Mining. pp. 420–428 (2020)
20. Mao, X., Wang, W., Xu, H., Wu, Y., Lan, M.: Relational reflection entity alignment. In: Proceedings of the 29th ACM International Conference on Information & Knowledge Management. pp. 1095–1104 (2020)
21. Mao, X., Ma, M., Yuan, H., Zhu, J., Wang, Z., Xie, R., Wu, W., Lan, M.: An effective and efficient entity alignment decoding algorithm via third-order tensor isomorphism. In: Proceedings of the 60th Annual Meeting of the Association for Computational Linguistics (Volume 1: Long Papers). pp. 5888–5898 (2022)
22. Mao, X., Wang, W., Wu, Y., Lan, M.: From alignment to assignment: Frustratingly simple unsupervised entity alignment. In: Proceedings of the 2021 Conference on Empirical Methods in Natural Language Processing. pp. 2843–2853 (2021)
23. Mao, X., Wang, W., Wu, Y., Lan, M.: Lightea: A scalable, robust, and interpretable entity alignment framework via three-view label propagation. In: Proceedings of the 2022 Conference on Empirical Methods in Natural Language Processing. pp. 825–838 (2022)
24. Maskey, S., Paolino, R., Bacho, A., Kutyniok, G.: A fractional graph laplacian approach to oversmoothing. arXiv preprint arXiv:2305.13084 (2023)
25. Pei, H., Wei, B., Chang, K.C.C., Lei, Y., Yang, B.: Geom-gcn: Geometric graph convolutional networks. In: International Conference on Learning Representations (2019)
26. Pei, S., Yu, L., Hoehndorf, R., Zhang, X.: Semi-supervised entity alignment via knowledge graph embedding with awareness of degree difference. In: The world wide web conference. pp. 3130–3136 (2019)
27. Rossi, E., Kenlay, H., Gorinova, M.I., Chamberlain, B.P., Dong, X., Bronstein, M.M.: On the unreasonable effectiveness of feature propagation in learning on graphs with missing node features. In: Learning on Graphs Conference. pp. 11–1. PMLR (2022)
28. Roth, A.E.: Deferred acceptance algorithms: History, theory, practice, and open questions. international Journal of game Theory **36**, 537–569 (2008)

29. Shi, X., Xiao, Y.: Modeling multi-mapping relations for precise cross-lingual entity alignment. In: Proceedings of the 2019 Conference on Empirical Methods in Natural Language Processing and the 9th International Joint Conference on Natural Language Processing (EMNLP-IJCNLP). pp. 813–822 (2019)
30. Sun, Z., Hu, W., Li, C.: Cross-lingual entity alignment via joint attribute-preserving embedding. In: The Semantic Web–ISWC 2017: 16th International Semantic Web Conference, Vienna, Austria, October 21–25, 2017, Proceedings, Part I 16. pp. 628–644. Springer (2017)
31. Sun, Z., Hu, W., Wang, C., Wang, Y., Qu, Y.: Revisiting embedding-based entity alignment: a robust and adaptive method. *IEEE Transactions on Knowledge and Data Engineering* (2022)
32. Sun, Z., Hu, W., Zhang, Q., Qu, Y.: Bootstrapping entity alignment with knowledge graph embedding. In: *IJCAI*. vol. 18 (2018)
33. Sun, Z., Huang, J., Hu, W., Chen, M., Guo, L., Qu, Y.: Transedge: Translating relation-contextualized embeddings for knowledge graphs. In: The Semantic Web–ISWC 2019: 18th International Semantic Web Conference, Auckland, New Zealand, October 26–30, 2019, Proceedings, Part I 18. pp. 612–629. Springer (2019)
34. Sun, Z., Wang, C., Hu, W., Chen, M., Dai, J., Zhang, W., Qu, Y.: Knowledge graph alignment network with gated multi-hop neighborhood aggregation. In: Proceedings of the AAAI conference on artificial intelligence. vol. 34, pp. 222–229 (2020)
35. Sun, Z., Zhang, Q., Hu, W., Wang, C., Chen, M., Akrami, F., Li, C.: A benchmarking study of embedding-based entity alignment for knowledge graphs. *Proceedings of the VLDB Endowment* **13**(12) (2020)
36. Trisedya, B.D., Qi, J., Zhang, R.: Entity alignment between knowledge graphs using attribute embeddings. In: Proceedings of the AAAI conference on artificial intelligence. vol. 33, pp. 297–304 (2019)
37. Wang, Y., Sun, H., Wang, J., Wang, J., Tang, W., Qi, Q., Sun, S., Liao, J.: Towards semantic consistency: Dirichlet energy driven robust multi-modal entity alignment. arXiv preprint arXiv:2401.17859 (2024)
38. Wang, Y., Cui, Y., Liu, W., Sun, Z., Jiang, Y., Han, K., Hu, W.: Facing changes: continual entity alignment for growing knowledge graphs. In: International Semantic Web Conference. pp. 196–213. Springer (2022)
39. Wang, Z., Lv, Q., Lan, X., Zhang, Y.: Cross-lingual knowledge graph alignment via graph convolutional networks. In: Proceedings of the 2018 conference on empirical methods in natural language processing. pp. 349–357 (2018)
40. Wang, Z., Yang, J., Ye, X.: Knowledge graph alignment with entity-pair embedding. In: Proceedings of the 2020 Conference on Empirical Methods in Natural Language Processing (EMNLP). pp. 1672–1680 (2020)
41. Wu, Y., Liu, X., Feng, Y., Wang, Z., Yan, R., Zhao, D.: Relation-aware entity alignment for heterogeneous knowledge graphs. In: Proceedings of the Twenty-Eighth International Joint Conference on Artificial Intelligence. International Joint Conferences on Artificial Intelligence (2019)
42. Wu, Y., Liu, X., Feng, Y., Wang, Z., Zhao, D.: Jointly learning entity and relation representations for entity alignment. In: Proceedings of the 2019 Conference on Empirical Methods in Natural Language Processing and the 9th International Joint Conference on Natural Language Processing (EMNLP-IJCNLP). pp. 240–249. Association for Computational Linguistics (2019)
43. Xu, C., Su, F., Lehmann, J.: Time-aware graph neural network for entity alignment between temporal knowledge graphs. In: Proceedings of the 2021 Conference on Empirical Methods in Natural Language Processing. pp. 8999–9010 (2021)

44. Xu, C., Su, F., Xiong, B., Lehmann, J.: Time-aware entity alignment using temporal relational attention. In: Proceedings of the ACM Web Conference 2022. pp. 788–797 (2022)
45. Xu, K., Song, L., Feng, Y., Song, Y., Yu, D.: Coordinated reasoning for cross-lingual knowledge graph alignment. In: Proceedings of the AAAI conference on artificial intelligence. vol. 34, pp. 9354–9361 (2020)
46. Xu, K., Wang, L., Yu, M., Feng, Y., Song, Y., Wang, Z., Yu, D.: Cross-lingual knowledge graph alignment via graph matching neural network. In: Proceedings of the 57th Annual Meeting of the Association for Computational Linguistics. pp. 3156–3161 (2019)
47. Ye, R., Li, X., Fang, Y., Zang, H., Wang, M.: A vectorized relational graph convolutional network for multi-relational network alignment. In: IJCAI. pp. 4135–4141 (2019)
48. Yu, D., Yang, Y., Zhang, R., Wu, Y.: Generalized multi-relational graph convolution network. arXiv p. 07331 (2020)
49. Zeng, K., Li, C., Hou, L., Li, J., Feng, L.: A comprehensive survey of entity alignment for knowledge graphs. *AI Open* **2**, 1–13 (2021)
50. Zeng, W., Zhao, X., Tang, J., Fan, C.: Reinforced active entity alignment. In: Proceedings of the 30th ACM International Conference on Information & Knowledge Management. pp. 2477–2486 (2021)
51. Zhu, Q., Wei, H., Sisman, B., Zheng, D., Faloutsos, C., Dong, X.L., Han, J.: Collective multi-type entity alignment between knowledge graphs. In: Proceedings of The Web Conference 2020. pp. 2241–2252 (2020)
52. Zhu, R., Ma, M., Wang, P.: Raga: relation-aware graph attention networks for global entity alignment. In: Pacific-Asia Conference on Knowledge Discovery and Data Mining. pp. 501–513. Springer (2021)

A Proof of Proposition 1

Proposition 1. (Existence of the solution.) The matrix Δ_{oo} is non-singular, allowing the reconstruction of other entity features \mathbf{x}_o using seed alignment entity features \mathbf{x}_s as $\mathbf{x}_o(t) = -\Delta_{oo}^{-1} \Delta_{os} \mathbf{x}_s$.

Proof. Initially, consider an undirected connected graph scenario where Δ_{oo} is a sub-matrix of the Laplacian matrix Δ . Given that sub-Laplacian matrices of undirected connected graphs are invertible [27], thus Δ_{oo} is non-singular. The spectral properties of eigenvalues in undirected graphs suggest similar non-singularity for directed graphs [24].

For general cases, assume an ordered representation of the adjacency matrix for a disconnected graph as:

$$\mathbf{A} = \text{diag}(\mathbf{A}_1, \dots, \mathbf{A}_r) \quad (27)$$

Here, $\mathbf{A}_i, i = 1, \dots, r$, represents each connected component. The gradient flow in equation (6) is applicable to each connected component independently for disconnected graphs. \square

B Proof of Proposition 2

Proposition 2. (Approximation of the solution.) With the iterative reconstruction solution as delineated in equation (10), and considering a sufficiently large iteration count N , the entity features will approximate the results of feature propagation as follows:

$$\mathbf{X}^{(N)} \approx \begin{pmatrix} \mathbf{x}_s \\ \Delta_{oo}^{-1} \tilde{\mathbf{A}}_{os} \mathbf{x}_s \end{pmatrix} \quad (28)$$

Proof. Commencing with the initial entity features $\mathbf{X}^{(0)}$ generated by EA encoders and applying equation (10), we iterate:

$$\begin{pmatrix} \mathbf{x}_s^{(k)} \\ \mathbf{x}_o^{(k)} \end{pmatrix} = \begin{pmatrix} \mathbf{I} & \mathbf{0} \\ \tilde{\mathbf{A}}_{os} & \tilde{\mathbf{A}}_{oo} \end{pmatrix} \begin{pmatrix} \mathbf{x}_s^{(k-1)} \\ \mathbf{x}_o^{(k-1)} \end{pmatrix} = \begin{pmatrix} \mathbf{x}_s^{(k-1)} \\ \tilde{\mathbf{A}}_{os} \mathbf{x}_s^{(k-1)} + \tilde{\mathbf{A}}_{oo} \mathbf{x}_o^{(k-1)} \end{pmatrix} \quad (29)$$

Given the stationary nature of the seed alignment entity features \mathbf{x}_s , we have the equation $\mathbf{x}_s^{(k)} = \mathbf{x}_s^{(k-1)} = \mathbf{x}_s$. The focus then shifts to the convergence of \mathbf{x}_o :

$$\mathbf{x}_o^{(k)} = \tilde{\mathbf{A}}_{os} \mathbf{x}_s + \tilde{\mathbf{A}}_{oo} \mathbf{x}_o^{(k-1)} \quad (30)$$

Expanding and analyzing the limit for the stationary state, we find:

$$\begin{aligned} \lim_{k \rightarrow \infty} \mathbf{x}_o^{(k)} &= \tilde{\mathbf{A}}_{os} \mathbf{x}_s + \lim_{k \rightarrow \infty} \sum_{i=2}^k \tilde{\mathbf{A}}_{oo}^{i-1} \tilde{\mathbf{A}}_{os} \mathbf{x}_s + \lim_{k \rightarrow \infty} \tilde{\mathbf{A}}_{oo}^k \mathbf{x}_o^{(0)} \\ &= \lim_{k \rightarrow \infty} \tilde{\mathbf{A}}_{oo}^k \mathbf{x}_o^{(0)} + \lim_{k \rightarrow \infty} \sum_{i=1}^k \tilde{\mathbf{A}}_{oo}^{i-1} \tilde{\mathbf{A}}_{os} \mathbf{x}_s \end{aligned} \quad (31)$$

Spectral graph theory provides critical insights into the properties of the Laplacian matrix Δ . It establishes that the eigenvalues of Δ are confined within the range $[0,2)$. This spectral characteristic has direct implications for the matrix $\tilde{\mathbf{A}} = \mathbf{I} - \Delta$, whose eigenvalues are consequently within the range $(-1,1]$. A pivotal aspect of this discussion, as elucidated in Proposition 1, is the non-singularity of Δ_{oo} . The absence of 0 as an eigenvalue of Δ_{oo} implies that $\tilde{\mathbf{A}}$'s eigenvalues strictly occupy the interval $(-1,1)$, thereby excluding the endpoints. This spectral behavior significantly influences the convergence properties of the iterative process. Specifically, the limit $\lim_{k \rightarrow \infty} \tilde{\mathbf{A}}_{oo}^n \mathbf{x}_o^{(0)}$ approaches 0. Furthermore, the summation $\lim_{k \rightarrow \infty} \sum_{i=1}^k \tilde{\mathbf{A}}_{oo}^{i-1}$ converges to $(\mathbf{I} - \tilde{\mathbf{A}}_{oo})^{-1} = \Delta_{oo}^{-1}$. By integrating these insights, the long-term behavior of the iterative solution can be articulated as:

$$\lim_{k \rightarrow \infty} \mathbf{x}_o^{(k)} = \Delta_{oo}^{-1} \tilde{\mathbf{A}}_{os} \mathbf{x}_s \quad (32)$$

Therefore, when the number of iterations N is sufficiently large, the entity features in $\mathbf{x}_o^{(N)}$ approximate $\Delta_{oo}^{-1} \tilde{\mathbf{A}}_{os} \mathbf{x}_s$. \square

C Alignment Search

In the testing process, rather than use the popular distance metric of Cross-domain Similarity Local Scaling (CSLS) [13] to search the alignments in most works, we follow [21] and [23] to formalize the entity alignment problem as an assignment problem to enforce the one-to-one alignment constraint. Before giving the mathematical definition, it assumes $|\mathcal{T}_s| = |\mathcal{T}_t| = n^t$ to simplify the process. In addition, it uses $SIM \in \mathbb{R}^{n^t \times n^t}$ to represent the cosine similarity matrix and compute it between testing entities in two \mathcal{KG} s with the entity embeddings. Thus, we attempt to solve the following optimization problem:

$$\arg \max_{P \in \mathbb{P}_{n^t}} \langle P, SIM \rangle \quad (33)$$

where \mathbb{P}_{n^t} is a set of permutation matrices with shape of $\mathbb{R}^{n^t \times n^t}$. Actually, we can directly obtain the optimal solution P^* by Sinkhorn operation [6].

$$P^* = \lim_{\tau \rightarrow 0^+} \text{Sinkhorn}\left(\frac{SIM}{\tau}\right) \quad (34)$$

where the operation of Sinkhorn is as follows:

$$\text{Sinkhorn}(\mathbf{X}) = \lim_{k \rightarrow +\infty} S^k(\mathbf{X}), S^k(\mathbf{X}) = \mathcal{N}_c(\mathcal{N}_r(S^{k-1}(\mathbf{X}))) \quad (35)$$

where $S^0(\mathbf{X}) = \exp(\mathbf{X})$, $\mathcal{N}_r(\mathbf{X}) = X \oslash (\mathbf{X} \mathbf{1}_{n^t} \mathbf{1}_{n^t}^\top)$ and $\mathcal{N}_c(\mathbf{X}) = X \oslash (\mathbf{1}_{n^t} \mathbf{1}_{n^t}^\top \mathbf{X})$ are the row and column-wise normalization operators of a matrix, \oslash denotes the element-wise division, $\mathbf{1}_{n^t}$ is a column vector of ones. Though we can only obtain an approximate solution with a small k in practice, we empirically found that

the approximate solution is enough to obtain a good alignment performance. Considering that the assumption of $n^t = |\mathcal{T}_s| = |\mathcal{T}_t|$ is easily violated, a naive reduction is to pad the similarity matrix with zeros such that its shape becomes $\mathbb{R}^{n^t \times n^t}$ where $n^t = \max(n_1^t, n_2^t)$.

D Datasets

We list the statistics of all datasets used in the experiments in Table 4.

Table 4: Statistics for datasets.

Datasets		Entity	Relation	Triple
DBP _{ZH-EN}	Chinese	19388	1701	70414
	English	19572	1323	95142
DBP _{JA-EN}	Japaense	19814	1299	77214
	English	19780	1153	93484
DBP _{FR-EN}	French	19661	903	105998
	English	19993	1208	115722
SRPRS _{FR-EN}	French	15000	177	33532
	English	15000	221	36508
SRPRS _{DE-EN}	German	15000	120	37377
	English	15000	222	38363

E Evaluation Metric

We utilize cosine similarity to calculate the similarity between two entities and employ H@k and MRR as metrics to evaluate all the methods. H@k describes the fraction of truly aligned target entities that appear in the first k entities of the sorted rank list:

$$H@k = \frac{1}{|S_t|} \sum_{i=1}^{|S_t|} \mathbb{I}[rank_i \leq k] \quad (36)$$

where $rank_i$ refers to the rank position of the first correct mapping for the i -th query entities and $\mathbb{I} = 1$ if $rank_i \leq k$ and 0 otherwise. S_t refers to the testing alignment set. MRR (Mean Reciprocal Ranking) is a statistical measure for evaluating many algorithms that produce a list of possible responses to a sample of queries, ordered by the probability of correctness. In the field of EA, the reciprocal rank of a query entity (i.e., an entity from the source KG) response is the multiplicative inverse of the rank of the first correct alignment entity in

the target KG. MRR is the average of the reciprocal ranks of results for a sample of candidate alignment entities:

$$MRR = \frac{1}{|S_t|} \sum_{i=1}^{|S_t|} \frac{1}{rank_i} \quad (37)$$